

# Microheater optimized for the integration with metasurface-based IR sources for gas sensing application

Costel PAUN<sup>1,2</sup>, Roxana TOMESCU<sup>1</sup>, Catalin PARVULESCU<sup>1</sup>, Octavian IONESCU<sup>1</sup>, Doina Elena GAVRILA<sup>3</sup>, and Dana CRISTEA<sup>1</sup>

<sup>1</sup>National Institute for Research and Development in Microtechnologies-IMT, 126A, Erou Iancu Nicolae Street, Bucharest, Romania

<sup>2</sup>Faculty of Electrical Engineering, University POLITEHNICA of Bucharest, Splaiul Independentei 313, Romania

<sup>3</sup>Faculty of Applied Sciences, University POLITEHNICA of Bucharest, Splaiul Independentei 313, Romania

E-mail: costel.paun@imt.ro

**Abstract.** This paper presents the design, manufacturing stages, electrothermal analysis and characterization of micro-heaters with platinum (Pt) resistive layer in four geometric configurations, which can be integrated with metasurfaces absorbers with applications in gas detection. The results obtained according to the electrothermal analysis and the performed experiments show that the studied micro-heaters can be integrated with metasurfaces to obtain the IR emission, necessary for gas detection.

**Key-words:** Microheater, IR emitter, metasurfaces, metamaterial absorber, gas sensor.

## 1. Introduction

Detection of toxic gases is an area of great relevance and interest. The surrounding atmosphere can contain various toxic gases that can be dangerous to humans, plants and animals.

A gas sensor that is part of a safety system converts chemical information into electrical signals (current, frequency, voltage).

In recent years, optical gas sensors based on the interaction of gas molecules with IR radiation have been intensively studied [1–4]. The principle of operation is based on the concentration-dependent absorption of the photons at specific gas wavelengths. Every gas has its own absorbing property to IR radiation with different wavelengths, and thus its unique IR absorption fingerprint [5]. These sensors offer advantages such as: stability, very good selectivity and sensitivity. The

IR source, which is an important component of these sensors should have a narrow emission wavelength bandwidth, adapted to the specific gas absorption spectra [2, 5].

The recently developed metasurfaces-based IR absorber/emitters showed the potential to become efficient quasi-monochromatic light sources and a cheaper alternative to the quantum cascade IR laser for sensing application [6–8]. This type of IR emitter is composed of a metal-dielectric-metal (MDM) metasurface with controlled spectral emissivity/absorptivity achieved with geometrically tuned electromagnetic resonances, and a broad-band IR source (e.g. a heater, usually an external one - Fig. 1). Plasmonic metasurfaces are a novel concept in nanophotonics having the role of tailoring the shape of the optical fields by using arrays of subwavelength resonators such as optical antennas [9, 10]. The MDM metasurface for the IR perfect absorbers/emitters consist in an array of sub-wavelength plasmonic structures, an insulator and a metal layer acting as a back-plane [8, 9]. The metasurface is designed to attain almost perfect absorption [10, 11] on narrow IR wavelength intervals specific for a certain gas. Kirchhoff law states that the emissivity of a material is equal to the absorption at equilibrium [11], so the metasurface based absorber can raise the emission at the desired wavelength, up to the level of an ideal blackbody.

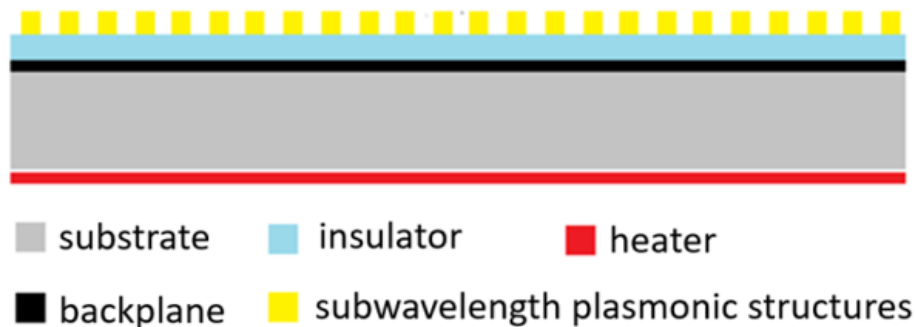


**Fig. 1.** Classic narrow band IR source based on metasurface.

Our aim is to develop a compact narrow-band IR source based on a broad-band infrared (IR) thermal source coupled with a narrow-band metasurface absorber. In this paper we focus on the development of the thermal source (heater) that can be easily integrated with the metasurface. The novelty of our approach consists in the integration of the thermal source (heater) with the metasurface, instead of using an external thermal source. Our new idea is to use the heater as a back-plane for the metasurface in order to miniaturize the device, to simplify the technology process, and to improve the heat transfer from the heater to the plasmonic structure. In addition, an amorphous silicon layer was added for further improvement of the heat transfer towards the plasmonic metasurface. Fig. 2 shows the proposed structure.

Microheaters based on materials such as poly-Si, TiN, SiC, Pt have been largely used in sensors that require operation at higher temperatures [12]. In this paper we present microheaters special designed to allow the integration with the multi-layer structure required for the narrow-band IR source. For this aim, the materials and geometry of the microheater assembly must be rigorously selected.

The characteristics of the microheater directly influence the performance of the gas sensor. The heater must develop a temperature at the desired level, and requires a low energy consumption, a short response time, and temperature distribution in the active area as uniform as possible.

[7, 8, 12]. The device was designed for CO<sub>2</sub> sensing applications. The target temperature is in the range 250-300°C necessary for a high emissivity of the metasurface in MWIR domain, with the peak centred at approx. 4.25 μm corresponding to a CO<sub>2</sub> absorption line [13].

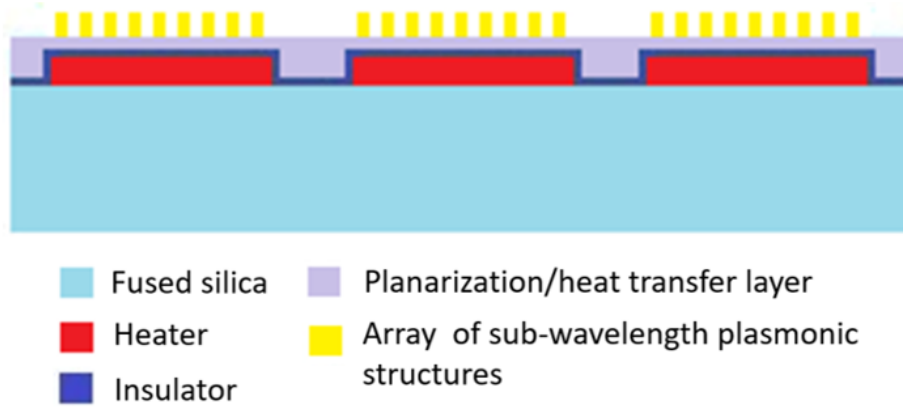


**Fig. 2.** Schematic of the proposed multi-layer structure for a narrow-band IR emitter.

This paper presents the design, manufacturing process and characterization of microheaters. This work is a follow-up of the paper [14], and presents detailed simulation results and characterization results using an improved characterization set-up that minimize the parasitic heat dissipation, and thus offering more accurate results.

## 2. Design and governing equations

The power dissipated in the resistive heater is:

$$P = RI^2 \quad (1)$$

where R is the resistance of the heating layer, and I is the current passing through it. The resistance value of the heating layer is given by:

$$R = \rho \frac{L}{w \cdot g} \quad (2)$$

where  $\rho$  is the material resistivity, L the length, w is the width, and g the thickness of the resistive layer. The generated resistive heat Q is given by:

$$\Delta Q = \Delta t \cdot P \quad (3)$$

where t is the time.

The heat produced by the Joule effect in the heating layer diffuses into the neighbouring layers and into the environment. Heat diffusion is achieved by conduction, convection and radiation. When the rate of heat production in the resistive layer is equal to the rate of heat dissipation through conduction ( $Q_{cond}$ ), convection ( $Q_{conv}$ ) and radiation ( $Q_{rad}$ ), the stable temperature of the microheater is reached.

$$\Delta t \cdot P = Q_{cond} + Q_{conv} + Q_{rad} \quad (4)$$

$$P = \frac{Q_{cond}}{\Delta t} + \frac{Q_{conv}}{\Delta t} + \frac{Q_{rad}}{\Delta t} \quad (5)$$

The rate of heat loss through conduction is given by eq. 6:

$$\frac{Q_{cond}}{\Delta t} = Ak \frac{\Delta T}{\Delta x} \quad (6)$$

where  $A$  is the area of the heat exchange surface,  $k$  is the coefficient of thermal conductivity,  $\Delta T$  the temperature difference between two opposite surfaces of the substrate, and  $\Delta x$  is the thickness of the material.

The rate of heat loss through convection is given by eq. 7:

$$\frac{Q_{conv}}{\Delta t} = A_s h \Delta T \quad (7)$$

where  $A_s$  denotes the area of the convection heat exchange surface,  $h$  is the convection heat transfer coefficient, and  $\Delta T$  is the temperature difference between the heater and the environment.

The rate of heat loss through radiation is:

$$\frac{Q_{rad}}{\Delta t} = A_R \varepsilon \sigma \Delta T^4 \quad (8)$$

where  $A_R$  is the area of the heat exchange surface by radiation,  $\varepsilon$  is the surface emissivity, and  $\sigma = 5.670 \times 10^{-8} \text{ W m}^{-2} \text{ }^\circ\text{C}^{-4}$  is the Stefan-Boltzmann constant. Equation (5) becomes:

$$P = Ak \frac{\Delta T}{\Delta x} + A_s h \Delta T + A_R \varepsilon \sigma \Delta T^4 \quad (9)$$

This mathematical formulation [15] governs the electro-thermal phenomenon studied below.

COMSOL Multiphysics software was used to simulate, model and design the structure of the microheater. In order to obtain the optimum geometry for the integrated microheater, several test simulations were performed. Based on a set of preliminary simulation four models of microheaters were selected: resistors with two meanders having a width of  $2490 \mu\text{m}$  (Fig. 3 a, b), and resistors with three meanders having a width of  $1660 \mu\text{m}$  (Fig. 3 c, d), each of them with either wide pads (Fig. 3 b, d), or narrow pads (Fig. 3 a, c).

The device active area of  $1 \text{ cm}^2$ . This large area was required by the existing experimental setup for the spectral characterization of the IR emitter. In the next steps the area will be minimized to reduce the power consumption.

The distance between the meanders is  $10 \mu\text{m}$  to minimize the area not covered by the metal layer, thus allowing the resistive element to act as a backplane as well.

The resistive layer of the microheater is made of Platinum layer  $80 \text{ nm}$  thick. Platinum has very good long-term stability, it is a chemically inert material, has a good thermal response at low powers, and the characteristic of resistivity depending on the temperature is linear.

For the heater substrate we choose fused silica due to its characteristics: high chemical resistance, high radiation resistance, low thermal conductivity, low thermal expansion, and high resistance to thermal shocks.

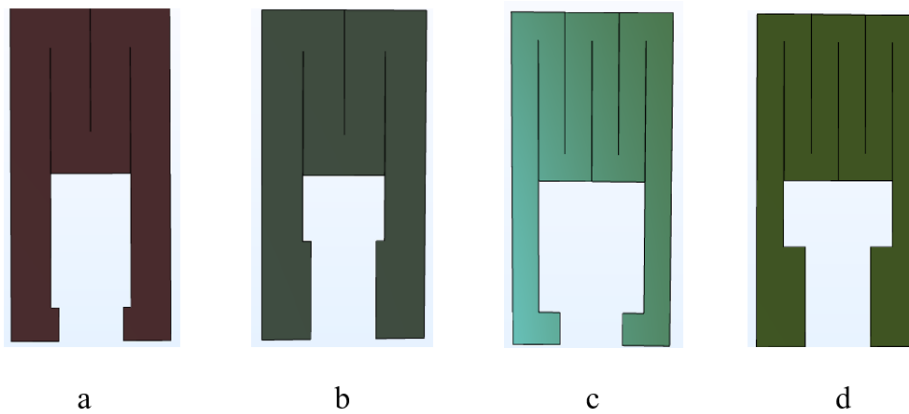


**Fig. 3.** Selected configurations of resistive microheaters: a) two meanders and narrow pad, b) two meanders and wide pad, c) three meanders and narrow pad, d) three meanders and wide pad.

The platinum layer is conformally covered with an insulating layer. We used  $\text{Al}_2\text{O}_3$ , as it is lossless around the wavelength of  $4.25\mu\text{m}$  corresponding to a  $\text{CO}_2$  absorption line. An amorphous silicon having high thermal conductivity layer is deposited on top, to facilitate the heat transmission from the heater to the plasmonic metasurface [16–18].

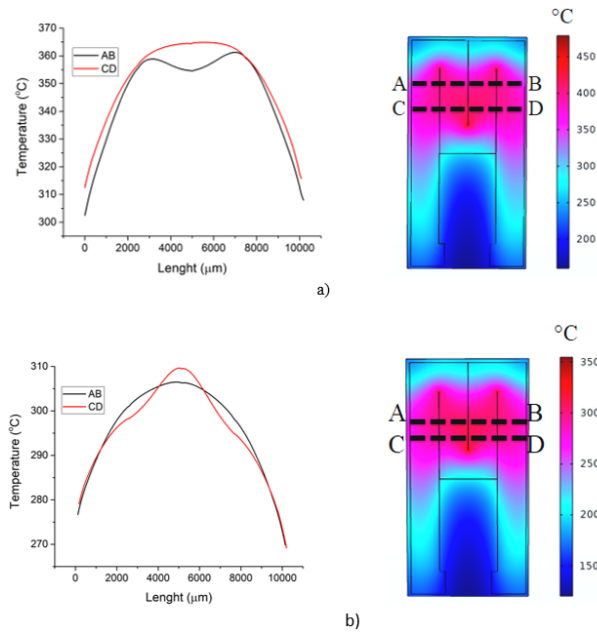
Electro-thermal simulations were performed to analyse the temperature distribution and to check if temperature of  $300^\circ\text{C}$  required for the optimal operation of the IR source at around  $4.25\mu\text{m}$  can be reached.

Table 1 illustrates the properties of the materials used in the electro-thermal simulation of the microheater.

**Table 1.**

Material Property at $20^\circ\text{C}$	Fused silica	Platinum	$\text{Al}_2\text{O}_3$	Silicon
Density [ $\text{Kg}/\text{m}^3$ ]	2200	21450	3965	2329
Electrical conductivity [ $\text{Kg}/\text{m}^3$ ]	$10^{-16}$	$8.9 \times 10^6$	0	$10^{-12}$
Heat capacity at constant pressure [ $\text{J}/\text{KgK}$ ]	703	133	730	700
Thermal conductivity [ $\text{W}/\text{mK}$ ]	1.3	71.6	35	130

Fig. 4-7 present the results of the electrothermal simulation for the four types of microheaters biased at 15 and/or 20 V. The temperature in the active area of the microheaters is scanned along the lines AB and CD to check the uniformity and the domain of the temperature that can be achieved in the different regions. According to the simulation results shown in Fig. 4-6 the four models of microheaters reach the optimum minimum operating temperature of the IR emitter ( $300^\circ\text{C}$ ). Higher temperatures at the same applied voltage are reached by the microheaters with two meanders (Fig. 4, 5). However, the microheaters with three meanders, and especially those with narrow pads show a better uniformity of the temperature over almost the entire active area (Fig.6).



**Fig. 4.** Temperature variation along the lines AB and CD at the surface of the microheater with two meanders and narrow pads: a) 20 V applied voltage; b) 15 V applied voltage.

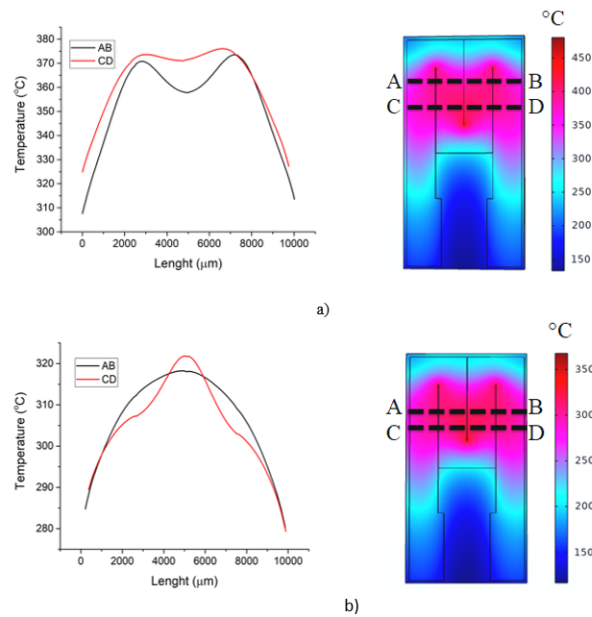


**Fig. 5.** Temperature variation along the lines AB and CD at the surface of the microheater with two meanders and wide pads: a) 20 V applied voltage; b) 15 V applied voltage.

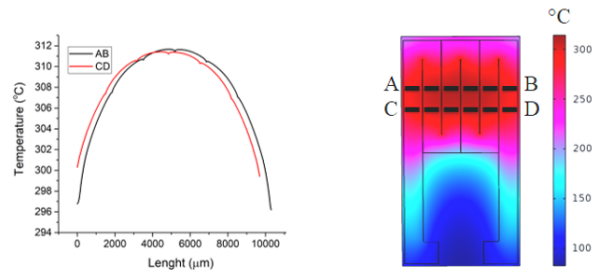


**Fig. 6.** Temperature variation along the lines AB and CD at the surface of the microheater with three meanders and narrow pads for 20 V applied voltage.

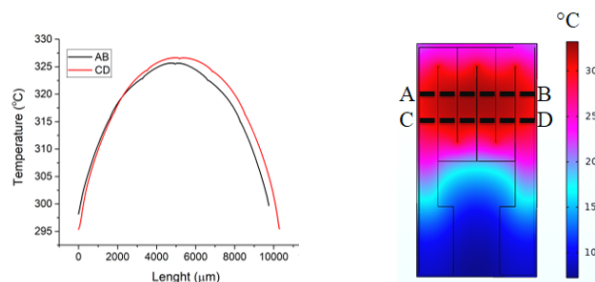


**Fig. 7.** Temperature variation along the lines AB and CD at the surface of the microheater with three meanders and wide pads.

Fig. 8 a and b show the temperature variation function on the applied voltage in the central area and in the pads area. One can see that the temperature in the pads area is significantly lower than the temperature in the central area for all types of microheaters, indicating that the pads design is adequate. The lowest temperature in the pads area can be obtained for the microheaters with three meanders and wide pads (Fig. 8b, blue curve).

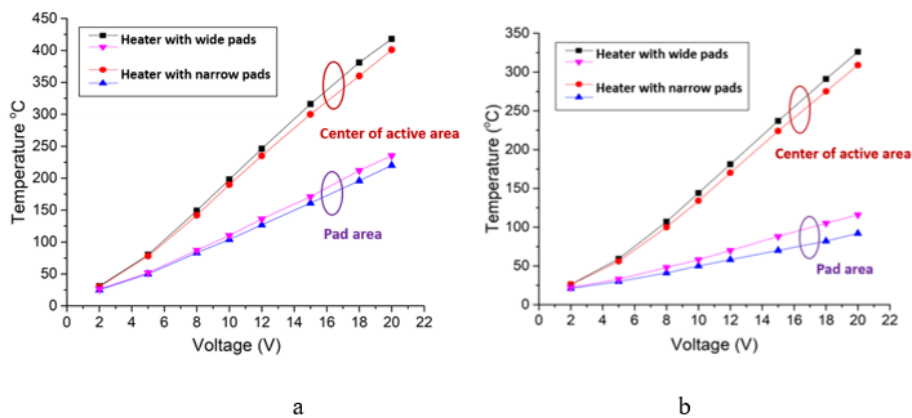


**Fig. 8.** Temperature variation function on the applied voltage in the central area, and in the pads area for: a) microheater with two meander - wide and narrow pads, b) microheater with three meanders wide and narrow pads.

### 3. Fabrication

Fig. 9 illustrates the main steps of the manufacturing process of the microheater. Fig. 9a - 9d and 9f - 9g show cross sections of the microheater in the active area of the meanders, while Fig. 9e presents a cross section through the pads' region.

The substrate is a fused silica wafer  $500\mu\text{m}$  thick (Fig.9a). The first important step is the deposition of the resistive layer (Pt) by e-beam evaporation followed by the patterning of the metal layer to obtain the resistor with the desired geometry (Fig. 9b). The patterning is achieved by using the lift-off technique. Then the  $\text{Al}_2\text{O}_3$  dielectric layer is deposited by the ALD (Atomic Layer Deposition) process (Fig. 9c). The next step is the deposition of the amorphous silicon layer using the sputtering method (Fig.9d). To open the pads, the photolithography and etching process through a photoresist mask of the amorphous silicon and  $\text{Al}_2\text{O}_3$  layers are performed (Fig.9e).

Above this multi-layered structure, the plasmonic structures for the metasurface are deposited and patterned using photo- or electron-beam lithography (Fig. 9f), metal deposition (Ti-Au), and lift-off process (Fig. 9g).

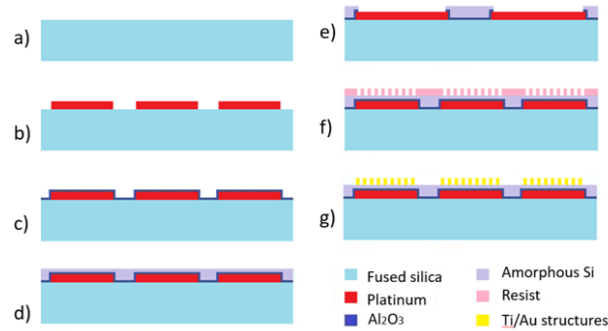


**Fig. 9.** Manufacturing processes: a) fused silica substrate; b) deposition and patterning of the Pt resistor; c)  $\text{Al}_2\text{O}_3$  deposition (ALD); d) amorphous silicon deposition (sputtering); e) opening of the pads (cross section through the area of the pads); f) resist deposition and lithography for lift-off; g) Ti-Au deposition and lift-off to obtain the micro/nanostructures for the metasurface.

### 4. Results and discussions

The Fig. 10 presents the resistance vs temperature characteristics of the microheaters. The microheaters were biased at 10 V, and placed on an electric hob in which the temperature varied from  $30^\circ\text{C}$  to  $310^\circ\text{C}$ . Using the voltage current characteristic, the resistance was calculated for the entire temperature range.

The results presented in Fig. 10 indicate that the function  $R(T)$  shows good linearity over the temperature range of interest.

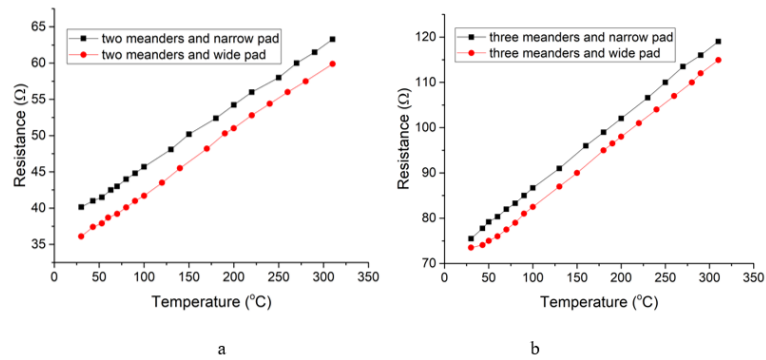


**Fig. 10.** Resistance vs temperature characteristics in the case of microheaters a) with two meanders b) with three meanders.

**A. Steady-state thermal analysis**

Temperature measurements were carried out with a temperature meter AX-5002 with a k-type thermocouple having an accuracy of 0.1% in the range  $-100...1300^{\circ}\text{C}$ . Non-contact measurements have been also performed using the IR camera FLIR 5000 SC calibrated with the k-type thermocouple.

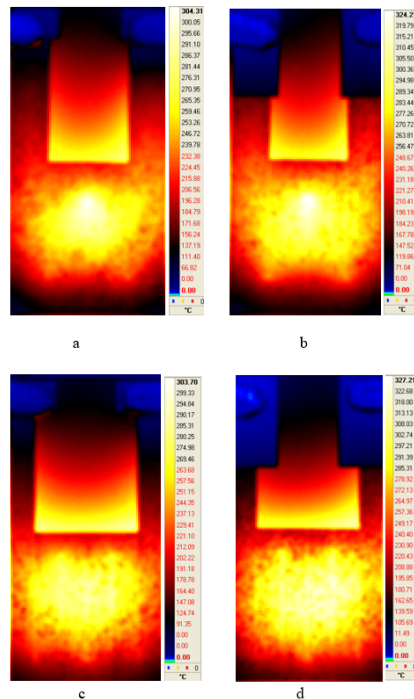


**Fig. 11.** The thermal images obtained with IR camera FLIR 5000 SC for the four heater geometries: a) two meanders and narrow pads, 15 V applied voltage, b) two meanders and wide pads 15 V applied voltage, c) three meanders and narrow pads, 20 V applied voltage d) three meanders and wide pads, 20 V applied voltage.

The images obtained with the IR camera, presented in Fig. 11, indicate a rather good uniformity in the central area of the heaters. As expected from the simulations, the temperature in the pads' area is much lower than the temperature in the central area, indicating that the length of the arms from the meanders to the pads is sufficient.

Fig. 12 shows the measured temperature variation on the applied voltage in the central area in comparison with the simulation results. The measurements were performed using the thermocouple contact method. One can see that the measurement results are in very good agreement with the simulations and all the microheaters can reach the required temperature domain at an applied voltage below 20V. The higher temperature at the same applied voltage is obtained with the microheaters with two meanders.

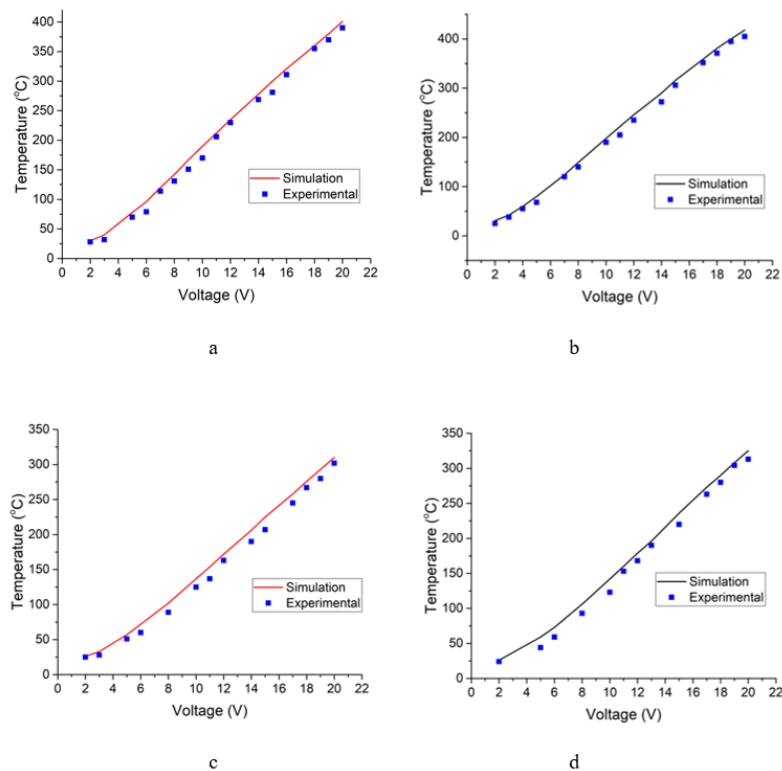


**Fig. 12.** Temperature vs voltage characteristic for the microheaters with: a) two meanders, narrow pad, b) two meanders, wide pad, c) three meanders, narrow pad, d) three meanders, wide pad.

### B. Transient thermal analysis

In this analysis, a voltage of 20 V is applied to the four heaters for 100 seconds. The thermal camera records the temperature during this time in the central point of the microheaters. Fig.13 presents the temperature variation in the analysed point for the four microheaters. According to these graphs, microheaters with wide pads have a shorter response time than those with narrow pads.

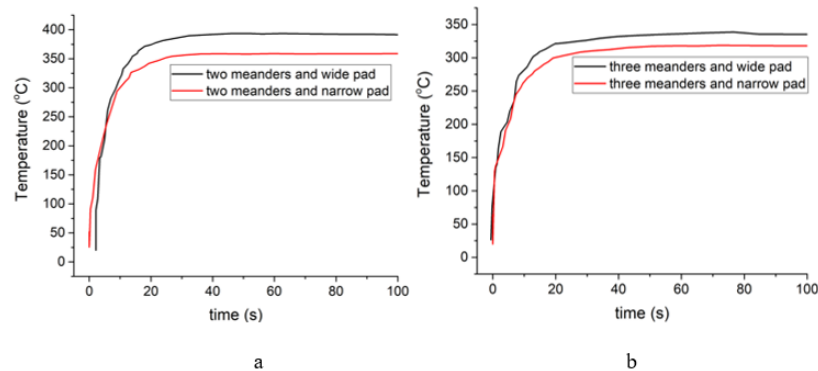


**Fig. 13.** Experimental transient analysis of microheaters for the four types of microheaters geometries: a) two meanders, b) three meanders.

## 5. Conclusions

Four types of microheaters designed for integration in a compact narrow band IR source based on plasmonic surfaces for gas sensing applications were developed and characterized.

The lay-out and the structure were optimized to simplify the structure of the integrated IR source, and to facilitate the heat transfer from the heater to the metamaterial absorber. The integrated heater plays a double role: wide band IR source and back-plane for the metasurface.

The characterization results indicate that the targeted temperature of 300°C required for the IR emitter for CO<sub>2</sub> sensor can be obtained in all four cases.

The higher temperatures at the same applied voltage can be obtained with the 2-meandre resistors. The microheaters with wide pads show a slightly better response time. The device will be further miniaturized to reduce power consumption and the response time.

**Acknowledgements.** This work was supported by a grant of the Romanian Ministry of Research and Innovation, CCCDIUEFISCDI, project number PN-III-P1-1.2-PCCDI-2017-0419/SENSIS P3 Infrared sensors for infrastructure security applications, within PNCDI III.

## References

- [1] LIU X., CHENG S., LIU H., HU S., ZHANG D., NING H., *A Survey on Gas Sensing Technology*, *Sensors* **12**, 9635–9665, 2012.
- [2] DINH T-V., IN-YOUNG CHOI I-Y., SON Y-S., JO-CHUN KIM J-C., *A review on non-dispersive infrared gas sensors: Improvement of sensor detection limit and interference correction*, *Sensors and Actuators B* **231**, pp.529–53, 2016.
- [3] HODGKINSON J., TATAM R.P., *Optical gas sensing: A review*. *Meas. Sci. Technol.* **24**, 012004, 2013.
- [4] D. POPA, F. UDREA, *Towards Integrated Mid-Infrared Gas Sensors*, *Sensors* **19**, 2076, 2019.
- [5] GORDON, I., *et al. The HITRAN2016 molecular spectroscopic database*. *J. Quant. Spectrosc. Radiat. Transf.* **203**, pp.3–69, 2017.
- [6] L. LA SPADA, *Metasurfaces for Advanced Sensing and Diagnostics*, *Sensors* **19**(2): 355, 2019.

- [7] LIAO Y-L., ZHAO Y., *Ultra-narrowband dielectric metamaterial absorber with ultrasparse nanowire grids for sensing applications*, Scientific Reports **10**:1480, 2020.
- [8] B-X. WANG, Y.HE, P.LOU, W.XING, *Design of a dual-band terahertz metamaterial absorber using two identical square patches for sensing application*, Nanoscale Advances **2**, pp.763–769, 2020.
- [9] COSTANTINI D., LEFEBVRE A., COUTROT A.-L., MOLDOVAN-DOYEN I., HUGONIN J.-P., BOUTAMI S., F.MARQUIER, BENISTY H., GREFFET J.-J., *Plasmonic Metasurface for Directional and Frequency-Selective Thermal Emission* Phys. Rev. Applied **4**, 014023, 014023, 2015.
- [10] YU N., CAPASSO F., *Flat optics with designer metasurfaces*. Nature Materials **13**, pp.139–150, 2014.
- [11] LIU X., TYLER T., STARR T., STARR A.F., JOKERST N.M., WILLIE J. PADILLA W.J., *Taming the Blackbody with Infrared Metamaterials as Selective Thermal Emitters*, Phys. Rev. Lett. **107**, 045901, 2011.
- [12] MAILLY F, *et. al.*, *Anemometer with hot platinum thin film*, Sensors and Actuators A: Physical **94**, pp.32–38, 2001.
- [13] TOMESCU R., *et.al*, *Control of IR emissivity with metasurface structures*, The 10th International Conference on Metamaterials, Photonic Crystals and Plasmonics META 2019, Lisbon. Portugal, July 23-26, 2019.
- [14] PAUN C., TOMESCU R., CRISTEA D., IONESCU O., PARVULESCU C, *Design, fabrication and characterization of a micro-heater for metasurface-based gas sensors*, Proc. of 2020 International Semiconductor Conference (CAS), 7-9 Oct. 2020, pp.31–34, 2020.
- [15] TIWARI, S.K., BHAT, S., MAHATO, K.K. *Design and fabrication of screen printed microheater*, Microsyst Technol **24**, pp.32733281, 2018.
- [16] FÜRJES P., DÜCSŐ C., ÁDÁM M., ZETTNER J., BÁRSONY I., *Thermal characterisation of microhotplates used in sensor structures*, Superlattices and Microstructures **35**, pp.455-464, 2004.
- [17] WU S., LIN Q., YUEN Y., TAI Y.C., *MEMS flow sensors for nano-fluidic applications*, Sensors and Actuators A: Physical **89**, pp. 152–158, 2001.
- [18] NOH S-S., SEO J-H., LEE E-A., *The fabrication by using surface MEMS of 3C-SiC micro-heaters and RTD sensors and their resultant properties*, Transactions on Electrical Electronic Materials **10**, pp.131–134, 2009.